PAPER

NJC
www.rsc.org/njc

Temperature dependence of the electronic ground states of two mononuclear, six-coordinate copper(II) centres

Malcolm A. Halcrow,*[a] Colin A. Kilner,[a] Joanna Wolowska,[b] Eric J. L. McInnes[b] and Adam J. Bridgeman*[c]

[a] *Department of Chemistry, University of Leeds, Woodhouse Lane, Leeds, UK LS2 9JT. E-mail: M.A.Halcrow@chem.leeds.ac.uk*
[b] *EPSRC CW EPR Service, Department of Chemistry, University of Manchester, Oxford Road, Manchester, UK M13 9PL*
[c] *Department of Chemistry, University of Hull, Kingston Upon Hull, U.K. HU6 7RX. E-mail: A.J.Bridgeman@hull.ac.uk*

Received* (in London, UK) *31st July 2003, Accepted 26th October 2003
First published as an Advance Article on the web 16th December 2003

Powdered $[Cu(L^2NH_2)_2][ClO_4]_2$ (**1**; L^2NH_2 = 2,6-bis{hydrazonomethyl}pyridine) and $[Cu(L^2OH)_2][ClO_4]_2$ (**2**; L^2OH = 2,6-bis{oximomethyl}pyridine) exhibit EPR spectra that are consistent with $\{d_{z^2}\}^1$ Cu(II) centres at 295 K. These slowly transform upon cooling to 5 K, to show *g*-values that more closely resemble $\{d_{y^2-z^2}\}^1$, pseudo-Jahn–Teller elongated structures. Single crystal X-ray structures of **1**·2$(CH_3)_2CO$ and **2**2$(CH_3)_2CO$ show the expected six-coordinate Cu(II) centres, with Cu–N bond lengths that are consistent with a $\{d_{z^2}\}^1$ configuration according to DF calculations. Importantly, the structure of **2** is temperature-dependent between 100–300 K, its Cu–N bond lengths varying in a manner consistent with the EPR data. The EPR spectra, and TLS analyses of the crystal structures, strongly imply that these changes are *not* a consequence of dynamic Jahn–Teller disorder. These results contrast with $[Cu(L^2Me)_2]^{2+}$ (L^2Me = 2,6-bis{*N*-methylcarbaldimino}pyridine) and other $[Cu(L^2R)_2]^{2+}$ complexes with small alkyl or aryl 'R' substituents, which adopt the more usual $\{d_{y^2-z^2}\}^1$ ground states at all temperatures.

Introduction

We have recently reported that distal substitution of the ligands L^1R and L^2R causes an unprecedented change in electronic ground state of the complexes $[Cu(L^1R)_2]^{2+}$ or $[Cu(L^2R)_2]^{2+}$, yielding a $\{d_{z^2}\}^1$ species in $[Cu(L^1Mes)_2]^{2+}$[1–3] and $[Cu(L^2tBu)_2]^{2+}$ (Scheme 1).[4] In contrast, the less hindered complexes $[Cu(L^1H)_2]^{2+}$,[1,2,5,6] $[Cu(L^2R)_2]^{2+}$ (R = Me, Cy)[4] and related complexes of Schiff base ligands with small distal substituents,[7] exhibit the more usual pseudo-Jahn–Teller-elongated $\{d_{y^2-z^2}\}^1$ ground state (Scheme 1). This phenomenon is caused by steric repulsion between the 'R' substituents of one coordinated L^1Mes or L^2tBu ligand and the pyridyl ring of the other, which causes an elongation of the four distal Cu–N bonds and leads to a molecular structure that is compressed along the N{pyridine}–Cu–N{pyridine} axis (Scheme 1). The same effect can be induced by ligand conformational strain in the $\{d_{z^2}\}^1$ complex $[Cu(L^3)_2]^{2+}$.[4] These compounds are the first authenticated examples of molecular six-coordinate Cu(II) complexes to possess a $\{d_{z^2}\}^1$ ground state,[8–10] although $KAlCuF_6$, which contains 1-D chains of vertex-sharing $[CuF_6]^{4-}$ distorted octahedra, also has this property.[11]

During this work, we noted a brief report that $[Cu(L^4)_2]Cl_2$ exhibits a $\{d_{z^2}\}^1$ EPR spectrum in solution;[12] although it had previously isolated by others,[13] no other spectroscopic or structural data have been reported for this compound. Since we had already shown that $[Cu(L^2Me)_2]^{2+}$ is a $\{d_{y^2-z^2}\}^1$ species,[4] this opened up the intriguing possibility that the ground state of the $[Cu(L^2R)_2]^{2+}$ centre might be controlled by the electron-withdrawing or -donating power of the L^2R 'R' substituent. While investigating that possibility, we have found that **1** and **2** appear to exhibit a uniquely temperature-dependent Jahn–Teller distortion, that is not connected with librational disorder of the copper coordination sphere.

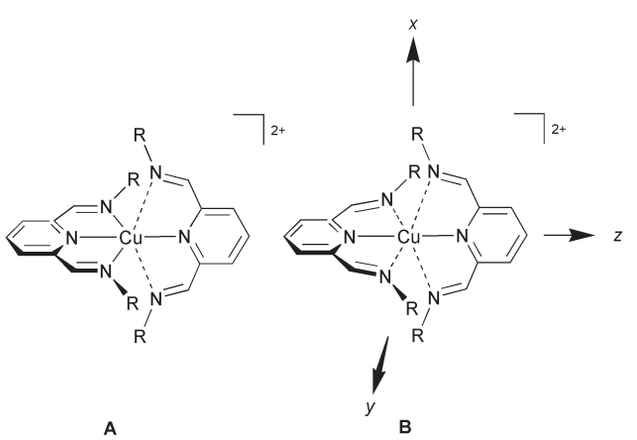

Scheme 1 Comparative molecular structures of $[Cu(L^2R)_2]^{2+}$ complexes with the ground states: (**A**) $\{d_{y^2-z^2}\}^1$; or (**B**) $\{d_{z^2}\}^1$.[4] The solid and dotted Cu–N bonds are short and long, respectively. The molecular axes of the $[Cu(L^2R)_2]^{2+}$ molecule used to derive these ground state labels are also shown.

Results and discussion

Complexation of Cu(II) salts by L^2NH_2 in organic solvents affords green solutions that turn dark brown over a period of minutes, from which only intractable oils can be isolated. By analogy with our earlier study of other $[Cu(L^2R)_2]^+$ and $[Cu(L^2R)_2]^{2+}$ derivatives, some of which also decompose in

DOI: 10.1039/b309071j

this way,[4] we believe that this reflects L^2NH_2-induced reduction of the Cu(II) content of the mixture to Cu(I) *in situ*. However, analytically pure olive-green microcrystals of $[Cu(L^2NH_2)_2][ClO_4]_2$ (**1**) can be precipitated from aqueous solutions of $CuCl_2$ and L^2NH_2, upon addition of excess $NaClO_4$. The isolated complex decomposes to a brown species after *ca.* 1 hour in organic solvents. However, **1** crystallises quite rapidly from acetone–Et_2O which, on one occasion, allowed a small number of single crystals to be grown (see below).

In contrast to **1**, lime green $[Cu(L^2OH)_2][ClO_4]_2$ (**2**) is indefinitely stable in organic solvents, and is most conveniently prepared by complexation of $Cu[ClO_4]_2{\cdot}6H_2O$ with 2 molar equivalents of L^2OH in acetone. Attempted preparations of **2** from aqueous solution in the manner analogous to **1** afforded soluble dark green material containing a sparingly soluble contaminant, that can be removed by recrystallisation from acetone–Et_2O. In agreement with a previous report,[14] this dark green byproduct analyses approximately as the neutral complex $[Cu(L^2OH)_2{-}2H]{\cdot}H_2O$ (found C, 40.8; H, 3.6; N, 20.1%: calcd, C, 41.0; H, 3.4; N, 20.5%). However, the FAB mass spectrum of this compound shows, in addition to the monocopper ions $[^{63}Cu(L^2OH)]^+$ ($m/z = 228$) and $[^{63}Cu(L^2OH)_2]^+$ (393) that are present in the spectrum of **2**, extra peaks corresponding to $[^{63}Cu_n(L^2OH)_n{-}(n+1)H]^+$ ($n = 2$, $m/z = 453$; $n = 3$, 682; $n = 4$, 909). These data suggest that solid "$[Cu(L^2OH)_2{-}2H]{\cdot}H_2O$" in fact contains a mixture of species.

The Q-band EPR spectra of solid, powdered **1** and **2** at 295 K are both rhombic and show similar *g*-values, with $g_1 > g_2 \gg g_3 \approx 2.00$ (Table 1). For **1** only, hyperfine coupling to $^{63,65}Cu$ is resolved on the g_3 component (Fig. 1). These spectra are clearly consistent with a $\{d_{z^2}\}^1$ ground state;[15,16] the large value of A_3 for **1**, and the fact that $g_3 \approx 2.00$ for both compounds, rule out the alternative interpretation that **1** and **2** contain fluxional $\{d_{y^2-z^2}\}^1$ Cu(II) centres.[10] Interestingly, however, both spectra are temperature-dependent, becoming more rhombic upon cooling. At 5 K, the spectrum of **1** clearly now shows $g_1 \gg g_2 > g_3 > 2.00$,[16] with *g*-values that are quite similar to those of $[Cu(L^2Cy)_2][BF_4]_2$ (**3**), which has a static $\{d_{y^2-z^2}\}^1$ configuration (Table 1, Fig. 1).[4] Hence, this compound apparently undergoes a transition from a $\{d_{z^2}\}^1$ ground state at room temperature, to a $\{d_{y^2-z^2}\}^1$ configuration at 5 K. The EPR spectrum of **2** at 5 K is apparently axial, but has an unusual line-shape that suggests contamination of the spectrum by intermolecular dipolar interactions.[15] Hence, while the apparent *g*-values of **2** are also temperature-dependent, the origin of this variation is less clear-cut than for **1**. At 110 and 5 K both **1** and **2** show a weak additional peak at $g = 2.19 \pm 0.01$ (Fig. 1), which is reproducible between samples and so is unlikely to be due to an impurity. We have previously reported a related compound, which crystallised as a mixture of static and fluxional $\{d_{y^2-z^2}\}^1$ Cu(II) centres and shows a similar feature at $g = 2.20$ in its EPR spectrum.[3] Hence, we tentatively suggest that the $g = 2.19$ signal in **1** and **2** arises from a small fraction of fluxional $\{d_{y^2-z^2}\}^1$ Cu(II) spins in these materials.

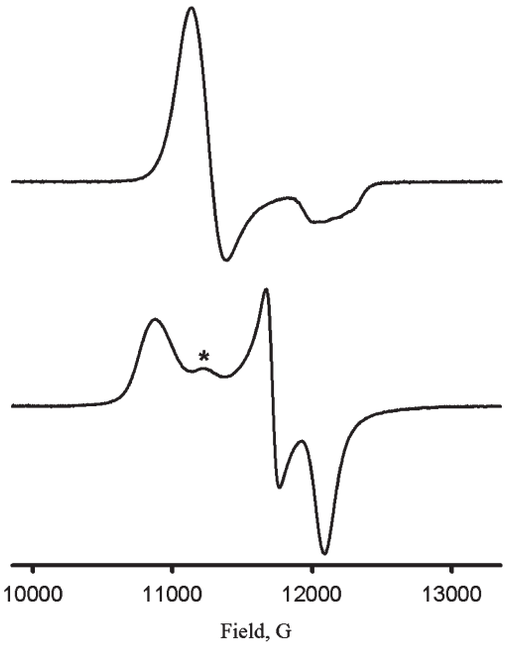

Fig. 1 Q-Band powder EPR spectra of **1** at 295 K (top) and 4 K (bottom). The starred feature may be due to a small fraction of fluxional Cu(II) centres in the sample – see text for details.

In 10 : 1 MeCN : toluene solution at 110 K, **1** and **2** show similar EPR spectra with no resolved hyperfine coupling. The spectrum for **2** is broader than for **1**, and apparently axial, but with a $g_\perp$ value that is within experimental error of the average of $g_1 + g_2$ for **1**. These spectra show somewhat different *g*-values compared to the powder spectra. In particular, the rhombic *g*-values for **1** are now closer to those of **3**; and, for both compounds $g_3 \approx 2.04$, which is more consistent with a $\{d_{y^2-z^2}\}^1$ Cu(II) centre. The visible spectra of both complexes in MeCN solution exhibit a single d–d maximum with no noticeable shoulders, at $\lambda_{max} = 681 \pm 1$ nm ($\varepsilon_{max} = 49$–62 $M^{-1}\,cm^{-1}$). This is consistent with the presence of near-homoleptic six-coordinate Cu(II) ions,[17] and is at only *ca.* 25 nm shorter wavelength than the d–d maxima shown by $[Cu(L^2R)_2][BF_4]_2$ (R = Me, Cy)[4] and related tridentate Schiff base complexes[7,18] in this or other solvents. The wavelength and intensity of this d–d peak in acetone are almost identical to that in MeCN, showing that the solution structures of **1** and **2** are not solvent-dependent. Hence, the six-coordinate structures of **1** and **2** are probably retained upon dissolution, but the EPR data suggest that the compounds may adopt a different electronic configuration in MeCN compared to the solid state.

We have been unable to grow solvent-free single crystals of either **1** or **2**. However, crystals of formula **1**·$2(CH_3)_2CO$ and **2**·$2(CH_3)_2CO$ were grown by diffusion of Et_2O vapour into acetone solutions of the complexes. Complex **1**·$2(CH_3)_2CO$ was analysed at 150 K. In the light of the temperature-dependent EPR spectra shown by **1** and **2**, **2**·$2(CH_3)_2CO$ was analysed at 100, 150 and 300 K. A variable temperature crystallographic study of **1** was not attempted, because of the

Table 1 *Q*-band EPR data for the Cu(II) complexes in this study. Selected data for $[Cu(L^2Cy)_2][BF_4]_2$ (**3**) and $[Cu(L^2tBu)_2][BF_4]_2$ (**4**), and calculated *g*-values for $[Cu(L^2R)_2]^{2+}$ (R = NH_2, $\mathbf{1}^{2+}$; R = OH, $\mathbf{2}^{2+}$; R = Me, $\mathbf{5}^{2+}$) are also included for comparison. Hyperfine couplings are to $^{63,65}Cu$ and are in G. Estimated errors on these parameters are $g \pm 0.002$, $A \pm 2$ G

	Phase	T/K	g_1	g_2	g_3	A_1	A_3
1	Powder	295	2.198	2.169	2.014	—	91
	Powder	110	2.238	2.104	2.034	—	—
	Powder	5	2.252	2.097	2.034	—	—
	MeCN	110	2.194	2.100	2.031	—	—
2	Powder	295	2.207	2.177	2.012	—	—
	Powder	110	2.225	2.159	2.008	—	—
	Powder	5[a]	2.230	2.103	2.103	—	—
	MeCN	110	2.151	2.151	2.039	—	—
3[b]	Powder	10	2.256	2.073	2.040	154	—
4[b]	Powder	10	2.219	2.219	1.998	—	161
$\mathbf{1}^{2+}$	Calcd.	—	2.113	2.080	2.004	—	—
$\mathbf{2}^{2+}$	Calcd.	—	2.114	2.075	2.007	—	—
$\mathbf{5}^{2+}$	Calcd.	—	2.117	2.042	2.031	—	—

[a] This spectrum has an unusual line-shape, and may be contaminated by intermolecular dipolar interactions. [b] Ref. 4.

difficulty in obtaining fresh single crystals of this material (see above). The Cu ions in both compounds have a very rhombic stereochemistry, with only small deviations from local C_{2v} symmetry (Figs. 2 and 3). The bond lengths and angles at Cu in **1** and **2** at 150 K are essentially identical (Table 2), and differ only in that the bonds Cu(1)–N(21) and Cu(1)–N(24) are slightly longer in **2** than in **1**, by an average of 0.031(6) Å. However, the structures of **2** at 300 and 150 K show clear differences. The bonds Cu(1)–N(9) and Cu(1)–N(12) become shorter upon cooling, from an average of 2.208(4) Å at 300 K to 2.161(2) Å at 150 K (Table 2). Correspondingly, Cu(1)–N(21) and Cu(1)–N(24) are lengthened from an average of 2.290(4) Å at 300 K to 2.329(2) Å at 150 K. The contraction of Cu(1)–N(9) and Cu(1)–N(12) appears to continue upon further cooling of **2** from 150 to 100 K (Table 2), although the difference is barely statistically significant. Precedent suggests that the bonds Cu(1)–N(9) and Cu(1)–N(12) should be most sensitive to the electronic ground state in **1** and **2**, and should take values near 2.05–2.10 Å for a compound adopting structure A, and 2.15–2.30 Å for structure B. Hence, the temperature-dependence of **2** is consistent with a gradual, but incomplete, change from a $\{d_{z^2}\}^1$ to a $\{d_{y^2-z^2}{}^2\}^1$ configuration between 300–100 K, as suggested by the EPR data.

Temperature-dependent structural changes of this type in crystalline six-coordinate Cu(II) compounds usually reflect dynamic disorder of a pseudo-Jahn–Teller axis of elongation between the different Cu–N bonds in the molecule.[8–10] This can be detected through a TLS analysis.[9,19] Importantly, the difference ($\langle d^2 \rangle$) between the mean-square displacement amplitudes (MSDAs)[9,19] for the Cu and N atoms of each Cu–N bond in **1**, and in **2** at all three temperatures, are $\leq 53 \times 10^{-4}$ Å^2 (Table 2). This strongly implies that the Cu ions in these structures have librationally ordered coordination spheres, since disordered Cu–N bonds generally give $\langle d^2 \rangle > 100 \times 10^{-4}$ Å^2.[20] Hence, the distribution of Cu–N bond lengths in **1** and **2** is not contaminated by Jahn–Teller disorder, and so is a true reflection of their molecular structures.[8–10]

The structures of **1**·2$(CH_3)_2$CO and **2**·2$(CH_3)_2$CO both show extensive intermolecular hydrogen-bonding within the crystal lattice. All 8 of the N–H donors in **1**·2$(CH_3)_2$CO are involved in intermolecular N–H···$OClO_3^-$, N–H···O=C$(CH_3)_2$ or N–H···NH_2 interactions. The NH_2 groups of one ligand in the complex, N(10) and N(13), each form one hydrogen bond to an acetone O atom, and one hydrogen bond to a NH_2 group of a neighbouring complex molecule. The NH_2 groups of the other ligand, N(22) and N(25), both donate hydrogen bonds to two different ClO_4^- anions. These interactions afford a 3-D hydrogen-bonded network of complex dications, linked by direct N–H···N contacts or through bridging ClO_4^- ions.

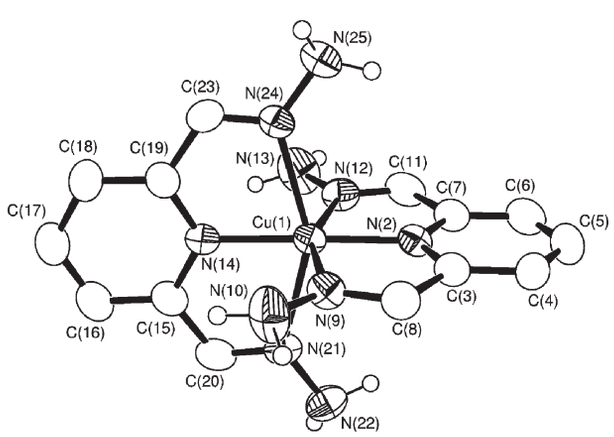

Fig. 2 View of the complex dication in the crystal structure of **1**·2$(CH_3)_3$CO. All C-bound H atoms are omitted for clarity. Thermal ellipsoids are at the 50% probability level.

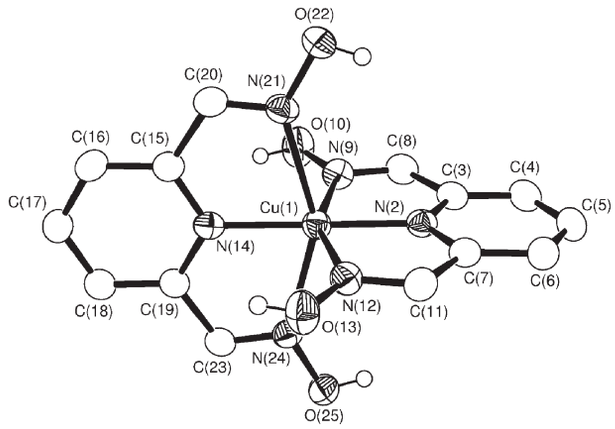

Fig. 3 View of the complex dication in the crystal structure of **2**·2$(CH_3)_3$CO at 150 K. All C-bound H atoms are omitted for clarity. Thermal ellipsoids are at the 50% probability level.

The hydrogen-bonding in **2**·2$(CH_3)_2$CO is related to that in **1**·2$(CH_3)_2$CO, but is much simpler. The OH groups on one ligand, O(10) and O(13), each form a O–H···O=C$(CH_3)_2$ hydrogen bond to of the two unique acetone molecules in the asymmetric unit. Those on the other ligand, O(22) and O(25), each form a O–H···$OClO_3^-$ interaction to a different anion. Hence, **2**·2$(CH_3)_2$CO exists as discrete, hydrogen-bonded $[Cu(L^2OH)_2][ClO_4]_2$·2$(CH_3)_2$CO super-molecules in the crystal.

In order to confirm our conclusions regarding the ground states of **1** and **2**, we performed static DFT calculations of the $[Cu(L^2NH_2)_2]^{2+}$ ($\mathbf{1}^{2+}$) and $[Cu(L^2OH)_2]^{2+}$ ($\mathbf{2}^{2+}$) dications, using the crystallographic atomic coordinates for these compounds at 150 K. For comparison, we also ran the same calculation on $[Cu(L^2Me)_2]^{2+}$ ($\mathbf{5}^{2+}$), using atomic coordinates derived from the crystal structure of **3**[4] but with the cyclohexyl 'R' substituents replaced by methyl groups. The ground state singly occupied molecular orbitals (SOMOs) derived from these calculations are shown in Fig. 4. As can be seen, the SOMO for $\mathbf{5}^{2+}$ has almost pure $\{d_{y^2-z^2}\}^1$ character, while those of $\mathbf{1}^{2+}$ and $\mathbf{2}^{2+}$ contain a substantial $\{d_{z^2}\}^1$ component. These results closely resemble those we have previously obtained from similar calculations of the ground states of $[Cu(L^1R)_2]^{2+}$ compounds,[2] and confirm our conclusions about the ground states of **1**–**3**.

Table 1 lists *g*-tensors for $\mathbf{1}^{2+}$, $\mathbf{2}^{2+}$ and $\mathbf{5}^{2+}$ calculated from the crystallographic coordinates, using the BP86 approach with the inclusion of spin–orbit coupling. *g*-Values of metal–organic d-electron radicals calculated by DF procedures are only qualitatively accurate.[21] Nonetheless, the results obtained in this study are in good agreement with the experimental trends in *g* between **1**–**3**. For $\mathbf{1}^{2+}$ and $\mathbf{2}^{2+}$, the calculated values show the clear trend $g_1 > g_2 \gg g_3 \approx g_e$, confirming the conclusion that these compounds show a predominantly $\{d_{z^2}\}^1$ ground state at 150 K. For $\mathbf{5}^{2+}$ the pattern $g_1 \gg g_2 > g_3 > g_e$ was calculated, with a g_3 of 2.03 that is close to the experimental value of 2.04. This pattern is more consistent with a $\{d_{y^2-z^2}\}^1$ Cu(II) centre.

We also performed DF geometry-minimisation calculations on $\mathbf{1}^{2+}$, $\mathbf{2}^{2+}$ and $\mathbf{5}^{2+}$, in order to see whether the *preference* of **1** and **2** for a $\{d_{z^2}\}^1$ configuration under certain conditions could be reproduced theoretically. However, all three dications minimised to pseudo-Jahn–Teller elongated $\{d_{y^2-z^2}\}^1$ molecular structures using LDA and BP86 approaches, with essentially identical coordination geometries at copper that resembled that of **3** in the crystal.[4] These may be an accurate reflection of the structures of **1**–**3** at 0 K in the gas phase. However, Jahn–Teller effects in transition ion compounds are known to be strongly dependent on molecular vibrational energies and the local molecular environment.[8,20] Hence it is likely that

Table 2 Selected bond lengths (Å) and angles (°) for **1**·2$(CH_3)_3CO$ at 150 K, and **2**·2$(CH_3)_3CO$ at three different temperatures. The square brackets contain values of $\langle d^2 \rangle$ (10^4 Å^2) calculated for the Cu–N bonds. A negative value of $\langle d^2 \rangle$ arises when MSDA(N) < MSDA(Cu)

		2		
	1	100 K	150 K	300 K
Cu(1)–N(2)	1.921(4) [18(20)]	1.9270(17) [39(9)]	1.9246(17) [46(9)]	1.933(3) [25(15)]
Cu(1)–N(9)	2.159(3) [25(18)]	2.1540(18) [19(9)]	2.1601(18) [21(10)]	2.211(3) [21(18)]
Cu(1)–N(12)	2.168(4) [50(19)]	2.1539(18) [30(9)]	2.1624(17) [22(9)]	2.205(3) [0(16)]
Cu(1)–N(14)	1.962(4) [53(19)]	1.9724(17) [38(8)]	1.9661(17) [42(8)]	1.958(3) [24(15)]
Cu(1)–N(21)	2.291(4) [34(19)]	2.3322(17) [6(9)]	2.3265(17) [−7(9)]	2.295(3) [5(17)]
Cu(1)–N(24)	2.305(3) [18(17)]	2.3315(17) [0(9)]	2.3322(17) [9(9)]	2.285(3) [30(17)]
N(2)–Cu(1)–N(9)	78.38(14)	77.74(7)	77.76(7)	77.14(12)
N(2)–Cu(1)–N(12)	78.14(15)	77.77(7)	77.64(7)	77.07(12)
N(2)–Cu(1)–N(14)	178.17(14)	178.69(7)	178.59(7)	178.85(11)
N(2)–Cu(1)–N(21)	103.40(15)	104.85(6)	104.75(6)	104.07(11)
N(2)–Cu(1)–N(24)	104.20(14)	104.00(6)	103.97(7)	104.11(11)
N(9)–Cu(1)–N(12)	156.52(16)	155.46(7)	155.36(7)	154.21(12)
N(9)–Cu(1)–N(14)	99.83(13)	100.96(7)	100.86(7)	101.73(11)
N(9)–Cu(1)–N(21)	90.14(13)	89.37(7)	89.73(7)	92.02(12)
N(9)–Cu(1)–N(24)	94.82(13)	95.66(6)	95.42(6)	93.78(11)
N(12)–Cu(1)–N(14)	103.64(15)	103.53(7)	103.76(7)	104.06(11)
N(12)–Cu(1)–N(21)	94.89(14)	95.34(6)	95.18(6)	93.89(11)
N(12)–Cu(1)–N(24)	91.28(13)	91.76(6)	91.81(6)	92.77(11)
N(14)–Cu(1)–N(21)	76.11(14)	75.23(6)	75.41(6)	75.69(11)
N(14)–Cu(1)–N(24)	76.28(14)	75.91(6)	75.86(6)	76.12(11)
N(21)–Cu(1)–N(24)	152.39(13)	151.13(6)	151.27(6)	151.81(11)

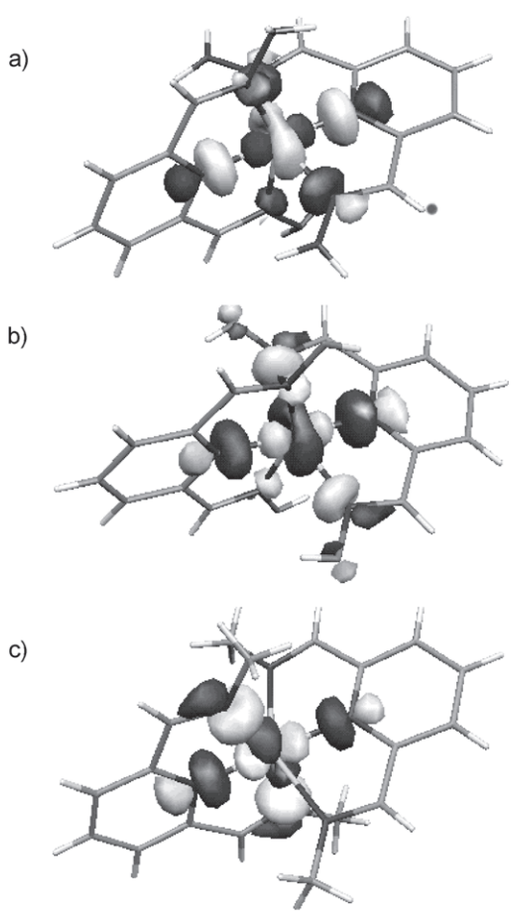

Fig. 4 Views of the calculated singly occupied molecular orbitals (SOMOs) for: a) $\mathbf{1}^{2+}$; b) $\mathbf{2}^{2+}$; and c) $\mathbf{5}^{2+}$.

theoretical models that take account of these, and other factors that influence molecular vibrations in condensed phases, will be needed to calculate the structural preferences of systems like the one in this study accurately and reliably.

Concluding remarks

This study has shown that the electronic structures of **1** and **2** are different in different phases of matter. As amorphous powders, the compounds show EPR spectra with similar *g*-values that are consistent with a $\{d_{z^2}\}^1$ ground state at 295 K, corresponding to structure B in Scheme 1. However, these spectra change significantly upon cooling. Although the spectra of **2** at lower temperatures are not clear-cut, the EPR behaviour of **1** clearly implies that its electronic configuration changes with temperature, from $\{d_{z^2}\}^1$ at 295 K to $\{d_{y^2-z^2}\}^1$ (structure A) at 5 K. This interpretation is supported by the crystal structures of **2**·2$(CH_3)_2CO$ at different temperatures, whose Cu–N bond lengths vary between 100–300 K in a manner consistent with a gradual change from structure B to structure A upon cooling. In agreement with the EPR data, the Cu–N distances at 100 K suggest that the transition is not complete at this temperature. In contrast, related six-coordinate Cu(II) compounds with temperature-independent $\{d_{z^2}\}^1$ and $\{d_{y^2-z^2}\}^1$ ground states by EPR, show crystallographic Cu–N bond lengths that do not change detectably upon cooling from 300–30 K.[3] Finally, in acetone solution **1** and **2** appear to retain their six-coordinate structures, and probably adopt a $\{d_{y^2-z^2}\}^1$ configuration (structure A).

An alternative, and more common, interpretation of these data might be that solid **1** and **2** adopt structure A and a $\{d_{y^2-z^2}\}^1$ configuration, with an axis of structural elongation that is dynamically disordered about the two N(imine)–Cu–N(imine) vectors in the molecules. That behaviour is exhibited by $[Cu(L^2Me)_2]^{2+}$ in the solid.[4] However, as discussed above the g_3 and *A* values from the powder EPR spectra of **1** and **2** at 295 K (Table 1) are inconsistent with a $\{d_{y^2-z^2}\}^1$ spin, while the small $\langle d^2 \rangle$ parameters calculated from the solvate crystal structures of **1** and **2** (Table 2) demonstrate the absence of dynamic *or* static librational disorder at their Cu(II) centres. All of this evidence argues in favour of our alternative interpretation, that the electronic configurations of solid **1** and **2** are temperature-dependent. That being the case, this is the first time that a temperature-dependent Jahn–Teller distortion, that is not connected with solid-state Jahn–Teller disorder, has been discovered in a molecular Cu(II) system.

Our cumulative work on the complexes $[Cu(L^1R)_2]^{2+}$, $[Cu(L^2R)_2]^{2+}$ and $[Cu(L^3)_2]^{2+}$ has shown that a $\{d_{z^2}\}^1$ ground state can be imposed on near-homoleptic six-coordinate Cu(II) complexes of meridianal tridentate ligands using: distal steric interactions;[1–4] conformational strain within the ligand backbone;[4] and, in this work, by inductively withdrawing distal ligand substituents. These results offer the possibility of controlling the ground state of an appropriate Cu(II) centre and allowing it to be switched in response to a stimulus. That is, a Cu(II) (or other Jahn–Teller-active ion) centre could be used as a reporter group for sensing applications. We are actively pursuing that possibility.

Experimental

All manipulations were performed in air using commercial grade solvents. 2,6-Bis(hydrazonomethyl)pyridine (L^2NH_2)[22] and 2,6-bis(oximomethyl)pyridine (L^2OH)[23] were prepared by the literature procedures, while $CuCl_2$, $Cu[ClO_4]_2{\cdot}6H_2O$ and $NaClO_4$ (Aldrich) were used as supplied. [**CAUTION**. While we have experienced no difficulty in handling **1** and **2**, metal–organic perchlorates are potentially explosive and should be handled with due care in small quantities].

Synthesis of bis[2,6-bis(hydrazonomethyl)pyridine]-copper(II) diperchlorate (1)

A mixture of $CuCl_2$ (0.10 g, 7.67×10^{-4} mol) and L^2NH_2 (0.25 g, 1.53×10^{-3} mol) in water (25 cm^3) was stirred with warming until all of the solid had dissolved. Addition of excess $NaClO_4$ (0.37 g, 3.02×10^{-3} mol) to this solution yielded an olive green microcrystalline precipitate which was filtered, washed with water and dried. The product was recrystallised from warm water. Yield 0.29 g, 64% (Found: C, 28.4; H, 3.2; N, 23.8; Calcd. for $C_{14}H_{18}CuCl_2N_{10}O_8$: C, 28.6; H, 3.1; N, 23.8%). FAB mass spectrum (fragment, %): 488 ($[^{63}Cu(L^2NH_2)_2(^{35}ClO_4)]^+$, 26), 389 ($[^{63}Cu(L^2NH_2)_2]^+$, 100), 325 ($[^{63}Cu(L^2NH_2)(^{35}ClO_4)]^+$, 34), 226 ($[^{63}Cu(L^2NH_2)]^+$, 73), 164 ($[HL^2NH_2]^+$, 18) with correct isotopic distributions. Selected IR data: 3375 m, 3293 m, 3210 m, 1635 w, 1600 m, 1552 m, 1070 vs, 932 w, 908 m, 890 m, 805 m, 722 m, 622 m cm^{-1}. UV/vis (CH_3CN): $\lambda_{max} = 233$ nm ($\varepsilon_{max} = 30\,300$ M^{-1} cm^{-1}), 252 (sh), 281 (37 200), 374 (12 300), 440 (sh), 682 (49). UV/vis ($\{CH_3\}_2CO$): $\lambda_{max} = 682$ ($\varepsilon_{max} = 54$ M^{-1} cm^{-1}).

Synthesis of bis[2,6-bis(oximomethyl)pyridine]copper(II) diperchlorate (2)

An acetone (25 cm^3) solution of $Cu[ClO_4]_2{\cdot}6H_2O$ (0.28 g, 7.57×10^{-4} mol) and L^2OH (0.25 g, $1.52\,10^{-3}$ mol) was stirred at room temperature for 15 min. The bright green solution was concentrated to *ca.* 5 cm^3, and filtered. Addition of excess diethyl ether to this solution yielded green microcrystals which were filtered, dried and analysed without further purification. Yield 0.30 g, 68% (Found: C, 28.5; H, 2.5; N, 14.3; Calcd. for $C_{14}H_{14}CuCl_2N_6O_{12}$: C, 28.4; H, 2.4; N, 14.2%). FAB mass spectrum (fragment, %): 492 ($[^{63}Cu(L^2OH)_2(^{35}ClO_4)]^+$, 10), 393 ($[^{63}Cu(L^2OH)_2]^+$, 100), 327 ($[^{63}Cu(L^2OH)(^{35}ClO_4)]^+$, 12), 228 ($[^{63}Cu(L^2OH)]^+$, 65), 166 ($[HL^2OH]^+$, 27) with correct isotopic distributions. Selected IR data: 3585 m, 3527 m, 3265 m, 1683 w, 1633 m, 1596 s, 1570 m, 1316 s, 1273 s, 1070 vs, 932 s, 803 s, 740 m, 688 s, 618 s cm^{-1}. UV/vis (CH_3CN): $\lambda_{max} = 228$ nm ($\varepsilon_{max} = 44\,000$ M^{-1} cm^{-1}), 252 (sh), 287 (16 200), 341 (4700), 435 (sh), 681 (62). UV/vis ($\{CH_3\}_2CO$): $\lambda_{max} = 680$ ($\varepsilon_{max} = 70$ M^{-1} cm^{-1}).

Single crystal X-ray structure determinations

Single crystals of formula **1**·2$(CH_3)_2CO$ and **2**·2$(CH_3)_2CO$ were grown by diffusion of diethyl ether vapour into solutions of the complexes in acetone. Experimental details from the structure determinations in this work are given in Table 3. All structures were solved by direct methods (SHELXS 97)[24] and refined by full matrix least-squares on F^2 (SHELXL 97).[25] Mean-square diplacement parameters were calculated using the program THMA11,[17] incorporated into the PLATON suite of crystallographic software.[26]

CCDC reference numbers 217086–217089. See http://www.rsc.org/suppdata/nj/b3/b309071j/ for crystallographic data in .cif or other electronic format.

X-Ray structure determination of 1·2$(CH_3)_2CO$. One ClO_4^- anion is disordered over two orientations in a 0.75 : 0.25 occupancy ratio, which share a common O atom. All Cl–O distances within this disordered anion were restrained to 1.43(2) Å,

Table 3 Experimental details for the single crystal structure determinations in this study

	1·2$(CH_3)_2CO$		**2**·2$(CH_3)_2CO$	
Formula	$C_{20}H_{30}Cl_2CuN_{10}O_{10}$	$C_{20}H_{26}Cl_2CuN_6O_{14}$	$C_{20}H_{26}Cl_2CuN_6O_{14}$	$C_{20}H_{26}Cl_2CuN_6O_{14}$
M_r	704.98	708.91	708.91	708.91
Crystal system	Monoclinic	Triclinic	Triclinic	Triclinic
Space group	*Cc*	$P\bar{1}$	$P\bar{1}$	$P\bar{1}$
a/Å	21.8166(4)	6.8580(2)	6.9012(2)	7.1602(1)
b/Å	7.3939(1)	13.0630(3)	13.1087(3)	13.2144(3)
c/Å	21.5138(3)	17.5689(5)	17.5759(4)	17.3567(3)
α/°	—	107.2649(14)	107.2644(16)	107.6773(12)
β/°	118.0158(7)	94.1119(11)	94.6164(16)	95.9665(13)
γ/°	—	105.6603(10)	105.2984(10)	103.6906(8)
V/Å^3	3063.71(8)	1427.36(7)	1442.66(6)	1492.58(5)
Z	4	2	2	2
μ/mm^{-1}	0.954	1.031	1.020	0.986
T/K	150(2)	100(2)	150(2)	300(2)
Measured reflections	25 996	24 468	25 848	23 705
Independent reflections	6988	6413	6541	6797
R_{int}	0.048	0.085	0.055	0.086
$R(F)^a$	0.049	0.039	0.037	0.063
$wR(F^2)^b$	0.138	0.114	0.100	0.198
Flack parameter	0.004(13)	—	—	—

^{a} $R = \Sigma[|F_o| - |F_c|]/\Sigma|F_o|$. ^{b} $wR = [\Sigma w(F_o^2 - F_c^2)/\Sigma wF_o^4]^{1/2}$.

and non-bonded O···O distances within a given disorder orientation to 2.34(2) Å. All non-H atoms except the minor anion disorder orientation were modeled anisotropically. All C-bound H atoms were placed in calculated positions; N-bound H atoms were initially placed in calculated positions, then allowed to refine freely with a common thermal parameter, subject to a restrained N–H distance of 0.92(2) Å and non-bonded 1,3-H···H distance of 1.50(2) Å. There are two residual electron density peaks of 1.2 *e* Å^{-3}, which in principle could correspond to *ca.* 0.15 of an O atom from a lattice water molecule. These residual peaks both lie $\leq$2.2 Å from other, fully occupied atoms in the lattice, however, which is too short to be a viable hydrogen-bonding distance. Hence, these two peaks were not included in the final model.

X-Ray structure determinations of 2·2(CH$_3$)$_2$CO. Three datasets were collected of this compound, at 100, 150 and 300 K. Different crystals were used for all three data collections. At 300 K, one of the two ClO_4^- anions was disordered, and was modelled using three orientations with a 0.20 : 0.40 : 0.40 occupancy ratio. All Cl–O distances within this disordered anion were restrained to 1.41(2) Å, and non-bonded O···O distances within a given disorder orientation to 2.30(2) Å. No disorder was detected during refinement of the 100 K and 150 K structures. All non-H atoms were modeled anisotropically, except for the disordered anion at 300 K. All C-bound H atoms were placed in calculated positions and allowed to refine using a riding model. The O–H groups in the 300 K structure were also treated in this way. However, at 150 K and 100 K the O-bound H atoms were located in the difference map, and allowed to refine freely with a common thermal parameter, subject to a restrained O–H distance of 0.79(2) Å.

Other measurements

Infra-red spectra were obtained as KBr disks in the range 400–4000 cm^{-1} using a Nicolet Avatar 360 spectrophotometer. UV/vis/NIR spectra were obtained with a Perkin-Elmer Lambda 900 spectrophotometer operating between 3300–200 nm, in 1 cm quartz cells. Positive ion fast atom bombardment (FAB) mass spectra were performed on a VG AutoSpec spectrometer, employing a 3-NOBA matrix. CHN microanalyses were performed by the University of Leeds Department of Chemistry microanalytical service. EPR spectra were obtained using a Bruker ESP300E spectrometer fitted with an ER5106QT resonator and ER4118VT cryostat. Spectral simulations were performed using in-house software which has been described elsewhere.[27]

All density functional (DF) calculations were performed using the ADF 2000.02 program.[28,29] Optimized geometries were obtained using the Vosko–Wilk–Nusair (VWN)[30] form of the local density approximation (LDA) and with Becke's 1988 exchange[31] and Perdew's 1986 correlation[32] (labelled BP86) corrections to the LDA. Slater type orbital (STO) basis sets of triple-ζ quality incorporating frozen cores and two polarization functions and the ZORA relativistic approach were used. EPR *g*-tensors were calculated using restricted BP86 calculations including spin–orbit coupling.

Acknowledgements

The authors thank Mr J. Friend (University of Manchester) for help with the EPR spectra, and Mr J. Elhaïk (University of Leeds) for help with the crystallographic data collection. Funding by The Royal Society (M.A.H.), the University of Hull and the University of Leeds is gratefully acknowledged.

References

1 N. K. Solanki, E. J. L. McInnes, F. E. Mabbs, S. Radojevic, M. McPartlin, N. Feeder, J. E. Davies and M. A. Halcrow, *Angew. Chem., Int. Ed.*, 1998, **37**, 2221.
2 A. J. Bridgeman, M. A. Halcrow, M. Jones, E. Krausz and N. K. Solanki, *Chem. Phys. Lett.*, 1999, **314**, 176.
3 N. K. Solanki, M. A. Leech, E. J. L. McInnes, J. P. Zhao, F. E. Mabbs, N. Feeder, J. A. K. Howard, J. E. Davies, J. M. Rawson and M. A. Halcrow, *J. Chem. Soc., Dalton Trans.*, 2001, 2083.
4 J. M. Holland, X. Liu, J. P. Zhao, F. E. Mabbs, C. A. Kilner, M. Thornton-Pett and M. A. Halcrow, *J. Chem. Soc., Dalton Trans.*, 2000, 3316.
5 M. A. Leech, N. K. Solanki, M. A. Halcrow, J. A. K. Howard and S. Dahaoui, *Chem. Commun.*, 1999, 2245.
6 N. K. Solanki, M. A. Leech, E. J. L. McInnes, F. E. Mabbs, J. A. K. Howard, C. A. Kilner, J. M. Rawson and M. A. Halcrow, *J. Chem. Soc., Dalton Trans.*, 2002, 1295; G. S. Beddard, M. A. Halcrow, M. A. Hitchman, M. P. de Miranda, C. J. Simmons and H. Stratemeier, *Dalton Trans.*, 2003, 1028.
7 C. Beguin, P. Chautemps, A. El Marzouki, J.-L. Pierre, S. M. Refaif, G. Serratrice, E. Saint-Aman and P. Rey, *J. Chem. Soc., Dalton Trans.*, 1995, 1939; A. J. Blake, A. J. Lavery and M. Schröder, *Acta Crystallogr., Sect. C*, 1996, **52**, 37; B. de Bruin, E. Bill, E. Bothe, T. Weyhermüller and K. Wieghardt, *Inorg. Chem.*, 2000, **39**, 2936.
8 M. A. Hitchman, *Comments Inorg. Chem.*, 1994, **15**, 197.
9 L. R. Falvello, *J. Chem. Soc., Dalton Trans.*, 1997, 4463.
10 M. A. Halcrow, *Dalton Trans.*, 2003, 4375.
11 G. Wingefeld and R. Hoppe, *Z. Anorg. Allg. Chem.*, 1984, **516**, 223; K. Finnie, L. Dubicki, E. R. Krausz and M. J. Riley, *Inorg. Chem.*, 1990, **29**, 3908; M. Atanasov, M. A. Hitchman, R. Hoppe, K. S. Murray, B. Moubaraki, D. Reinen and H. Stratemeier, *Inorg. Chem.*, 1993, **32**, 3397; V. M. Masters, M. J. Riley and M. A. Hitchman, *J. Synchrotron Rad.*, 1999, **6**, 242.
12 Y. Nishida, K. Ida and S. Kida, *Inorg. Chim. Acta*, 1980, **38**, 113.
13 J. D. Curry, M. A. Robinson and D. H. Busch, *Inorg. Chem.*, 1967, **6**, 1570.
14 J. Pinart, C. Petitfaux and J. Faucherre, *Bull. Soc. Chim. Fr.*, 1974, 1781.
15 F. E. Mabbs, *Chem. Soc. Rev.*, 1993, 313.
16 B. A. Goodman and J. B. Raynor, *Adv. Inorg. Chem.*, 1970, **13**, 135.
17 A. B. P. Lever, *Inorganic Electronic Spectroscopy*, 2nd edn., Elsevier, Amsterdam, 1984, pp. 554–572.
18 P. H. Merrell, E. C. Alyea and L. Ecott, *Inorg. Chim. Acta*, 1982, **59**, 25.
19 J. D. Dunitz, V. Schomaker and K. N. Trueblood, *J. Phys. Chem.*, 1988, **92**, 856.
20 B. J. Hathaway, *Struct. Bonding (Berlin)*, 1984, **57**, 55.
21 See *e.g.* F. Neese and E. I. Solomon, *Inorg. Chem.*, 1998, **37**, 6568; S. Patchovskii and T. Ziegler, *J. Chem. Phys.*, 1999, **111**, 5730; E. van Lenthe, A. van der Avoird, W. R. Hagen and E. J. Reijerse, *J. Phys. Chem. A*, 2000, **104**, 2070; K. M. Neyman, D. I. Ganyushin, A. V. Matveev and V. A. Nasluzov, *J. Phys. Chem. A*, 2002, **106**, 5022.
22 R. C. Stoufer and D. H. Busch, *J. Am. Chem. Soc.*, 1956, **78**, 6016.
23 B. H. Kim, E. J. Jeong, G. T. Hwang and N. Venkatesan, *Synthesis*, 2001, 2191.
24 G. M. Sheldrick, *Acta Crystallogr., Sect. A*, 1990, **46**, 467.
25 G. M. Sheldrick, SHELXL 97, *Program for the Refinement of Crystal Structures*, University of Göttingen, Germany, 1997.
26 A. L. Spek, PLATON, *A multipurpose crystallographic tool*, Utrecht University, Utrecht, the Netherlands.
27 F. E. Mabbs and D. Collison, *Electron Paramagnetic Resonance of d Transition Metal Compounds*, Elsevier, Amsterdam, 1992, ch. 7.
28 ADF2000.02, E. J. Baerends, D. E. Ellis and P. Ros, *Chem. Phys.*, 1973, **2**, 41; L. Versluis and T. Ziegler, *J. Chem. Phys.*, 1988, **88**, 322; G. te Velde and E. J. Baerends, *J. Comput. Phys.*, 1992, **99**, 84; C. Fonseca Guerra, J. G. Snijders, G. te Velde and E. J. Baerends, *Theor. Chem. Acc.*, 1998, **99**, 391.
29 G. te Velde, F. M. Bickelhaupt, E. J. Baerends, G. Fonseca Guerra and T. Ziegler, *J. Comput. Chem.*, 2001, **22**, 931.
30 S. H. Vosko, L. Wilk and M. Nusair, *Can. J. Phys.*, 1980, **58**, 1200.
31 A. D. Becke, *Phys. Rev. A*, 1988, **38**, 3098.
32 J. P. Perdew, *Phys. Rev. B*, 1986, **33**, 8822.